THE JOURNAL OF PHYSICAL CHEMISTRY C

pubs.acs.org/JPCC Article

Direct Imaging of Precursor Adcomplex States during Cryogenic-Temperature On-Surface Metalation: Scanning Tunneling Microscopy Study on Porphyrin Array with Fe Adsorption at 78.5 K

Eiichi Inami,* Masataka Yamaguchi, Ryohei Nemoto, Hideki Yorimitsu, Peter Krüger, and Toyo Kazu Yamada*

Cite This: J. Phys. Chem. C 2020, 124, 3621−3631 Read Online

ACCESS | Metrics & More | Article Recommendations | Supporting Information

ABSTRACT: On-surface metalation of metal-free π-conjugated planar molecules, such as metal-free tetraphenylporphyrin (2HTPP), using 3d transition metals prepared in ultrahigh vacuum (UHV), attracted significant attention as a newly developed bottom-up method to create a building block for 1-nm-size nano devices, one- or two-dimensional nano networks, as a precursor of further on-surface synthesis or a magnetic atom array aligned on a well-ordered molecular template with an extreme low impurity concentration. Experimental and theoretical studies for this type of on-surface metalation via dehydrogenation (e.g., 2HTPP + Fe → H_2 + FeTPP) have been successfully demonstrated by depositing 3d metal atoms on metal-free π-conjugated planar molecular array at 300 K with subsequent annealing of 350−700 K in UHV. Significantly, photoemission spectroscopy study for the on-surface metalation process at cryogenic temperatures suggested a precursor adcomplex state different from the normal metalation state. In this study, we demonstrate that on-surface metalation at cryogenic temperature reduces thermal diffusion of both metal atoms and molecules, which allows gentle adsorption of the 3d metal atoms inside the molecule, providing precursor adcomplex states while preserving the original well-ordering molecular array structure. Using scanning tunneling microscopy (STM) we investigated Fe deposition on a well-ordered metal-free tetraphenylporphyrin (2HTPP) monolayer array islands with an Au(111) substrate temperature maintained at 78.5 K. Through direct STM topographic and spectroscopy imaging supported by density functional theory calculations, we identify three types of TPP appearance: (1) original 2HTPP, (2) 2HTPP with an Fe atom on top (precursor adcomplex "α" state), and (3) 2HTPP with an Fe atom inside (precursor adcomplex "γ" state, where a clear LUMO peak change was observed).

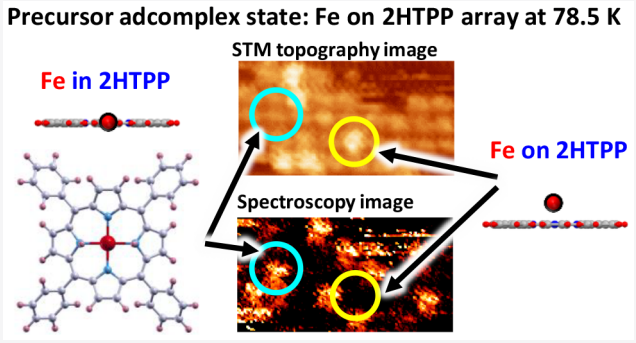

1. INTRODUCTION

On-surface metalation of metal-free π-conjugated planar molecules, such as porphyrins (TPP) or phthalocyanines (Pc), with 3d transition metal adsorption has attracted research attention as an excellent method to create well-ordered magnetic molecular nanostructures where planar molecules serve as hosts for metal atoms (see ref 1 and references therein).

Obtained metal−molecule complexes via on-surface metalation play an important role in extreme miniaturization of functional units and their atomically precise bottom-up fabrication process toward future high-functional devices. For this task, increasing attention focuses on porphyrin [see Figure 1] and similar planar π-conjugated molecules as promising building blocks to self-assemble well-ordered one- or two-dimensional templates,[2,3] which allow us to design supramolecular architectures.[4,5] The synthesized metal−molecule complexes exhibit tremendous diversity in physical/chemical properties based on the guest metal species and thus provide a vast range of functionalities such as chemical sensor,[6−11] catalysts,[12−15] solar cells,[16−18] and information storage devices.[19−22]

Conventionally, metal−molecule complexes synthesized via ex-situ methods including chemical reactions in solvents[23−25] and physical vapor deposition[26−29] are drop-casted on various substrates and form a well-ordered self-assembly molecular monolayer film in air at room temperature. Alternatively, on-surface metalation is a newly developed approach where guest metal atoms are deposited on the preadsorbed molecules on atomically flat and cleaned noble metal substrates, which realize an extremely low impurity concentration because all in situ growth and metalation processes are performed in

Received: October 18, 2019
Revised: January 21, 2020
Published: January 23, 2020

https://dx.doi.org/10.1021/acs.jpcc.9b09795
J. Phys. Chem. C 2020, 124, 3621−3631

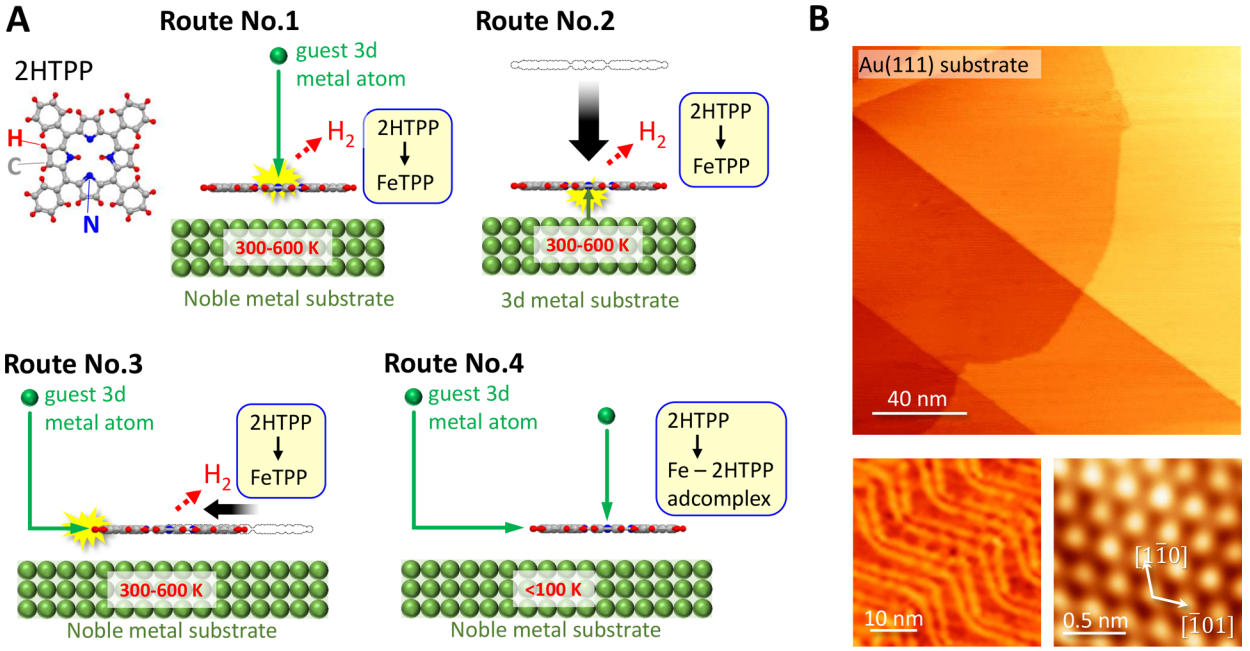

Figure 1. (A) Schematic illustration of typical reaction routes for metalation of metal-free tetraphenylporphyrin (2HTPP) molecules with an adsorption of guest metal atoms or substrate metal atoms. (B) STM topography images obtained on a clean Au(111) surface at 78.5 K. Upper panel: 164 × 164 nm^2, V_s = −300 mV, and I_t = 50 pA. Right-lower panel: Au(111) surface reconstruction pattern, 40 × 40 nm^2, V_s = −1400 mV, and I_t = 500 pA. Left-lower panel: Au atoms, 1.5 × 1.5 nm^2, V_s = −70 mV, and I_t = 100 pA.

ultrahigh vacuum (UHV). Furthermore, even metal organic molecules that are highly reactive at ambient pressure, e.g., FePc,[30−33] can be used in UHV as building blocks to create a clean molecular monolayer film.

On-surface metalation also stimulated fundamental research of chemical reactions. Specifically, scanning tunneling microscopy (STM) is used to reduce the problem of complicated interactions between huge amounts of molecules and metal atoms to single-molecule level. Hence, in situ metalations on several metal surfaces are examined via extensive STM studies, such as direct imaging,[34−40] spectroscopy,[2,41] and manipulation,[33,42,43] which unveiled reaction routes between single molecules and metal atoms and characterized a variety of metal−molecule complexes.

In the aforementioned studies (see, e.g., ref 1 and references therein), the metalations proceeded on a surface maintained at room temperature or higher and typically required substrate temperatures of 300−700 K. With respect to the well-ordered molecular monolayer film, two possible metalation processes are reported (see Figure 1A). The one is direct contact of 3d metal atoms on the preadsorbed target molecule [route no. 1 in Figure 1A][34,38,39,44−46] where the metal atoms were evaporated from the evaporator located in UHV chamber. The other is the interaction of molecule with the substrate 3d metal atom (see route no. 2 in Figure 1A).[39,47] For both route no. 1 and route no. 2, X-ray photoelectron spectroscopy (XPS) clearly showed that additional annealing at 350−700 K stimulates a chemical reaction; e.g., 2HTPP + Fe → FeTPP + H_2 (gas).[1]

Previously, it was demonstrated that metalation can be achieved with precise control of the amount of deposited 3d metal by using well-ordered arrays of planar molecules.[1,44−46] For example, fcc-Au(111) is composed of 1387 Au atoms in a 10 × 10 nm^2 area. When metal-free tetraphenylporphyrin (2HTPP) molecules are adsorbed on the Au(111) surface, they form a 1.4 nm × 1.4 nm square lattice, meaning only 51 molecules are enough to cover the 10 × 10 nm^2 area. If one 2HTPP captures one 3d metal atom during the metalation, only 0.037 (=51/1387) monolayers (ML) of 3d metal deposition is enough to change all 2HTPP to 3d-TPP.

However, when more than 0.037 ML of 3d metal was deposited at 300 K, the excess metal atoms play extra roles[34] since they thermally diffuse along the surface. For example, Fe or Co atoms on noble metal surfaces are known to diffuse to form triangular islands at room temperature.[20,48,49] Also, molecular diffusion should be considered in the case of molecular nanoisland. For example, a previous STM study indicated that the metal-free tetraphenylporphyrin (2HTPP) monolayer islands on Au(111) surface vary over time at the edge parts owing to thermal diffusion of individual molecules at room temperature.[3] These types of high-mobility metal atoms and molecules should react with each other via in-plane lateral interaction [see route no. 3 in Figure 1A],[42] and thus they can form a variety of metal−molecules complexes. Importantly, this type of metalation can destroy well-ordered molecular structures due to multiple routes of metalation process. For example, an STM study of the metalation of *meso*-tetramesitylporphyrin island on Cu(100) with 0.1−0.3 monolayers (ML) of Fe adsorption at room temperature, where hundreds of Fe atoms were deposited on about 50 molecules, demonstrated how the generation of Fe islands and Fe−porphyrin complex clusters causes disorder of the film structure.[34] Also, a 0.1 ML Fe deposition on a well-ordered metal-free phthalocyanine (H_2Pc) monolayer film at 300 K in UHV destroyed the original molecular lattice and produced Fe−molecule nanoclusters (see Supporting Information, Figure S5).

On-surface metalation processes (route nos. 1−3) at 300 K with sufficient annealing (350−700 K) produce a change the 2HTPP to 3d-TPP. However, another type of on-surface

https://dx.doi.org/10.1021/acs.jpcc.9b09795
J. Phys. Chem. C 2020, 124, 3621−3631

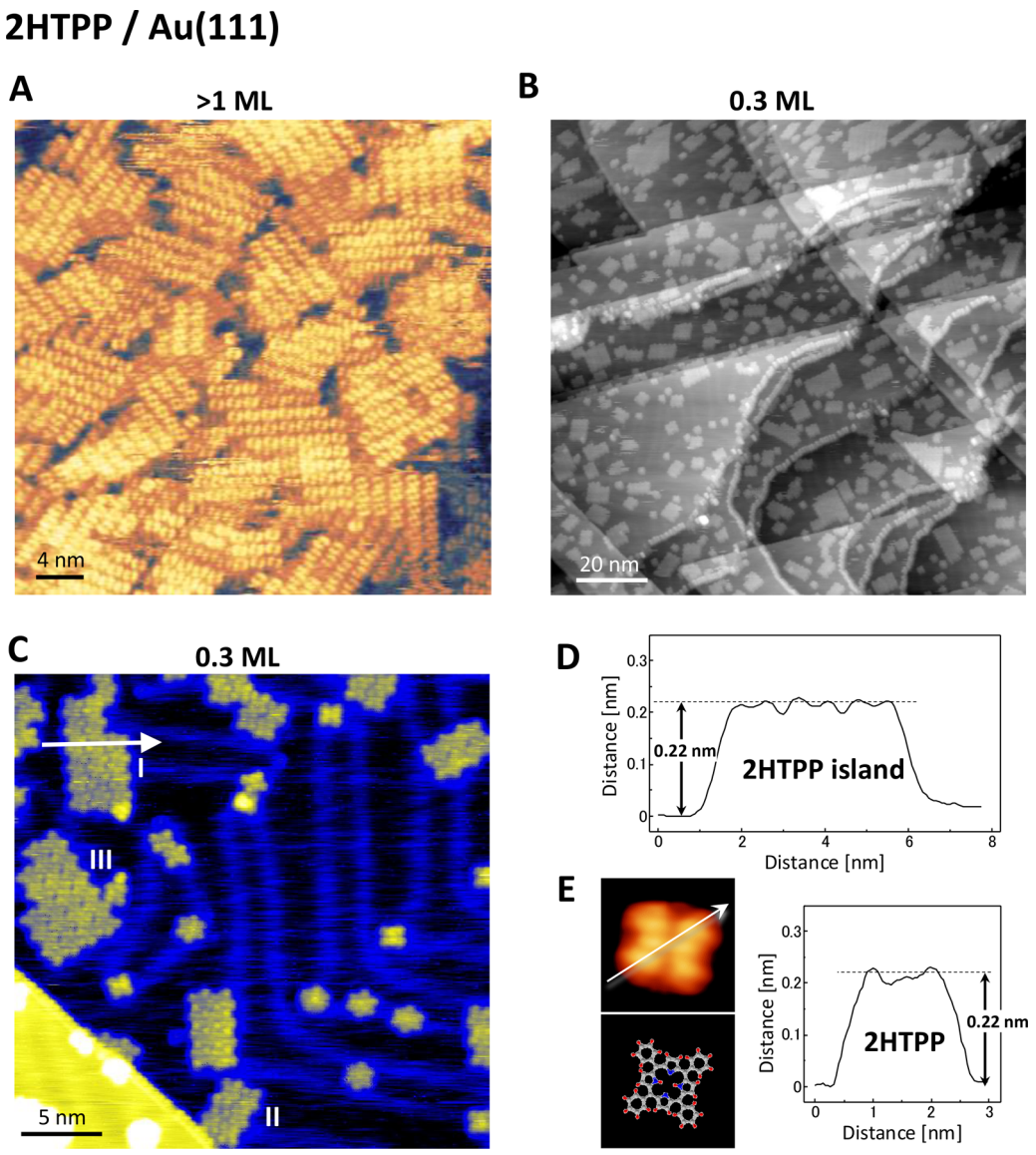

Figure 2. 2HTPP monolayer islands and single molecules grown on Au(111) at 300 K. STM images are obtained at 78.5 K in UHV. Deposition amounts of 2HTPP are (A) > 1 ML and (B and C) 0.3 ML. (A) 39 × 39 nm^2, V_s = +1000 mV, and I_t = 10 pA, (B) 130 × 130 nm^2, V_s = −1400 mV, and I_t = 10 pA. (C) 46 × 46 nm^2, V_s = −1400 mV, and I_t = 10 pA. In part C, three types of islands are shown, which are rotational symmetries of each other. (D) Height profile along the white arrow in part C. (E) Left panels: STM image of single 2HTPP molecule (top) and the corresponding molecular model (bottom). Right panel: height profile along the white arrow in the left panel.

metalation was reported from XPS and calculation studies of 3d metals of Fe and Co atoms deposited on the 2HTPP films at cryogenic temperature (100 K).[44,50] It was found that the metal atom inserted inside the 2HTPP is coordinated to the two iminic nitrogen atoms, while the two hydrogen atoms are still bonded to the two aminic nitrogen atoms, which is called a precursor adcomplex state [route no. 4 in Figure 1A].

In this study, we show first real space imaging on the surface of the precursor adcomplex state of the on-surface metalation process by means of a home-built low-temperature (78.5 K) UHV STM setup. About 100 Fe atoms were deposited on about 50 2HTPP per 30 × 15 nm^2 area (6243 Au atoms located) at the substrate temperature maintained at 78.5 K. Supported by density functional theory, our STM topographic and spectroscopy images reveal three different TPP appearances: (1) original 2HTPP, (2) 2HTPP with an Fe atom on top (precursor adcomplex "α" state), and (3) 2HTPP with an Fe atom inside (precursor adcomplex "γ" state; a clear LUMO peak change was observed).

Further, we have succeeded in maintaining the original well-ordered molecular structures even when depositing more Fe atoms than the numbers of preadsorbed 2HTPP owing to cryogenic temperature where in-plane mobilities of both adsorbed molecules and metal atoms are considerably decreased.

2. METHODS

2.1. UHV-LT-STM Setup. On-surface metalation of metal-free tetraphenylporphyrin (2HTPP) monolayer islands on Au(111) was demonstrated with 3d-metal adsorption at room temperature and liquid nitrogen temperature of 78.5 K in UHV via a home-built low-temperature UHV-STM setup (base pressure <8 × 10^{-9} Pa).[51] Our system included an introduction, a preparation, and an STM analytical chamber.

https://dx.doi.org/10.1021/acs.jpcc.9b09795
J. Phys. Chem. C 2020, 124, 3621−3631

They were interconnected for performing sample preparations and their STM characterization without breaking UHV. The STM stage in the analytical chamber was surrounded by a cryostat, where two Cu shields (Au-coated) cut heart radiation. The sample was placed on the outer cooling shield for 15 min, and then set into the STM head by opening the outer and inner shield doors shortly. The head was kept at 78.5 K by filling the liquid nitrogen in the cryostat bath inner (8 L) and outer (17 L) tanks (CryoVac Co. Ltd.). Typically, we waited for 2−3 h to cool both tip and sample to 78.5 K. Subsequently, the W tip was approached and scanned the sample surface.

2.2. Sample Preparations. As a metal substrate, Au(111) was subjected to several cycles of Ar^+ ion sputtering (1 kV) and annealing at 873 K in the preparation chamber by which a clean and atomically flat surface, including herringbone reconstruction,[52,53] was obtained (see Figure 1B).

The growth of the 2HTPP submonolayer films was performed using homemade molecular evaporator set in the preparation chamber. 2HTPP was purchased from TCI and was chromatographically purified on silica gel (Wako gel C-200) with a mixture of dichloromethane and hexane (v/v = 1:1) as an eluent. The eluent containing 2HTPP was evaporated under a reduced pressure on a rotary evaporator. The 2HTPP thus obtained was further purified by sublimation in vacuum (~10^{-4} Pa). Recrystallized 2HTPP powders (5−10 mg) were set into the crucible. Powdered 2HTPP in an Al_2O_3 crucible was heated to 423 K over 1 h for degassing and then deposited on the Au(111) substrate maintained at room temperature for 198 s (~0.3 ML 2HTPP) in the preparation chamber. After the deposition, the substrate was moderately annealed at 373 K for 5 min to facilitate the film formation with well-ordered square islands via self-assembly [same as Figure 2].

The cobalt deposition at 300 K was performed as follows. In the preparation chamber, ~0.28 ML cobalt (Co) was deposited at 300 K from the evaporator (Co rod: purity 99.95%). With respect to iron deposition at 78.5 K, iron (Fe rod: purity 99.995%) was evaporated from a multisource evaporator set in the STM analytical chamber. The outlet of the evaporator points toward the sample located on the STM stage. We opened the cooling shield door only 5 s to deposit only small amounts of Fe (approximately 0.02 ML, corresponding to about 100 atoms per 30 × 15 nm^2 area).

2.3. STM Characterization. The STM measurements were performed at 78.5 K. Electrochemically etched W-tip (ϕ = 0.3 mm, purity 99.99%) was carefully cleaned via annealing in the introduction chamber prior to utilization[54] and then subsequently set into the STM stage. The STM topographic images were obtained in a constant current mode. Sample local density of states (LDOS) was investigated via current imaging tunneling spectroscopy (CITS) measurement. In the CITS, topography and current−voltage characteristics (I−V) were recorded at each pixel. Each I−V spectrum was numerically differentiated to obtain differential conductance (dI/dV) curves and dI/dV maps, where dI/dV is considered as proportional to LDOS.[55] Therefore, the obtained data enabled a direct comparison of the topography and LDOS in the same area. Specifically, dI/dV values at positive and negative voltage sides denote unoccupied and occupied LDOS, respectively, near the Fermi energy (E_F).

2.4. Density Functional Theory Calculations. We have computed the structure and electronic states of 2HTPP, Fe-2HTPP adcomplex, and FeTPP single molecules [see Figure 5B and Supporting Information, Figures S3 and S4], using density functional theory (DFT) with the PBE exchange-correlation potential and the VASP software.[56] For Fe-2HTPP and FeTPP, DFT+U was used with U = 4 eV and J = 1 eV for the Fe d states. Previously, these values were found to give the best results for various Fe−porphyrin molecules.[57] The energy cutoff was set to 400 eV, and the simulation box was 20 × 20 × 14 Å. The atomic positions were fully optimized until the forces on all atoms were smaller than 0.01 eV/Å. Fe-2HTPP and FeTPP are in an intermediate spin (S = 1) state.

3. RESULTS AND DISCUSSION

3.1. 2HTPP Monolayer Islands on Au(111). Figure 2 shows STM topographic images obtained on the Au(111) atomic terraces after deposition of >1 ML [Figure 2A] and 0.3 ML [Figure 2, parts B and C] of 2HTPP molecules. Most of the adsorbed molecules formed well-ordered rectangular-shaped islands on the surface via self-assembly when the 2HTPP single molecules touch down on Au(111) at 300 K with subsequent annealing at 373 K. Currently, we focused on the submonolayer regime. Figure 2C shows an enlarged image (46 nm × 46 nm) where approximately 10 square monolayer islands were placed on the (111) terrace while some molecules remained isolated or aligned (trapped) along the step edges. Figure 2D shows the height profile across one molecular island [white arrow in Figure 2C], thereby revealing the apparent height from the Au(111) substrate corresponding to approximately 0.22 nm, which is identical to the single 2HTPP height shown in Figure 2E. The heights were comparable with the monolayer height.[3] Additionally, it was possible to identify that the 2HTPP films were rotated by 120° relative to each other as labeled by type-I, type II, and type III in Figure 2C. Statistical analysis of the images surveyed over 250 nm × 250 nm area confirmed that given 740 2HTPP islands in total, the ratios of type-I, type II, and type III islands corresponded to 29%, 38%, and 33%, respectively. The result suggested that the three types were energetically equivalent, and their rotational differences were simply due to 3-fold symmetry of the Au(111) surface.[3]

3.2. Cobalt Deposition at 300 K on 2HTPP Array. The previously reported photoemission spectroscopy and STM studies demonstrated successful on-surface metalation by depositing 3d metal atoms on a π-conjugated molecular monolayer array at 300 K with subsequent annealing at 350−700 K.[1] However, in this process, the number of deposited 3d atoms should not exceed the number of preadsorbed molecules. If it does, the original well-ordered molecular structures can be disordered at 300 K. Indeed, the reported STM study directly indicated that the adsorption of 0.1−0.3 monolayers of Fe at 300 K deconstructed well-ordered *meso*-tetramesitylporphyrin islands on Cu(100) to generate Fe islands and isolated Fe−porphyrin complex clusters.[34] In that case, hundreds of Fe atoms were deposited on 51 molecules in a 10 × 10 nm^2 area. We also demonstrated that well-ordered metal-free phthalocyanine (H_2Pc) monolayer film was destroyed by a 0.1 ML Fe deposition at 300 K in UHV and Fe−molecule nanoclusters were grown (see Supporting Information, Figure S5).

To ensure the occurrence of the aforementioned type of a disordering process due to 3d-atom metalation for other systems, we examined 0.28 ML cobalt deposition on a 0.3 ML 2HTPP array wherein the substrate was maintained at 300 K. Figure 3A shows the resulting STM image (40 × 40 nm^2), in

https://dx.doi.org/10.1021/acs.jpcc.9b09795
J. Phys. Chem. C 2020, 124, 3621−3631

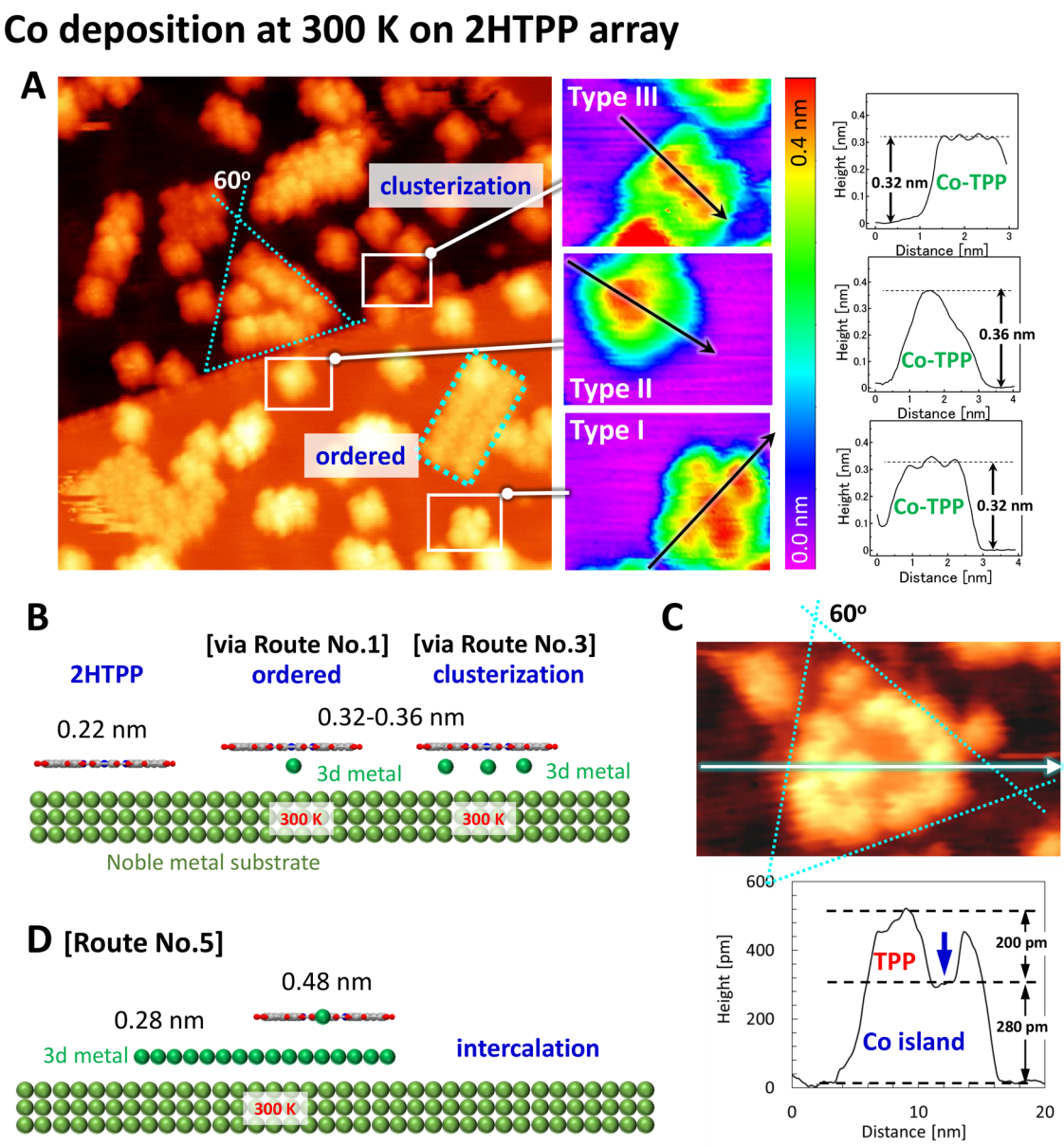

Figure 3. Co deposition at 300 K on 2HTPP array in UHV. STM images are obtained at 78.5 K. (A) STM topography image: 40 × 40 nm^2, V_s = −1400 mV, and I_t = 30 pA. Three types of single molecules induced by Co deposition were marked by white boxes in (A). Height profiles of these three types of isolated complexes are shown in the right panels. (B) Schematic illustration of two possible reaction routes of Co-2HTPP complexes. Ordered complexes are produced via route no. 1, while the isolated clusters were grown via route no. 3. (C) Upper panel: STM image of triangular-shaped intercalated Co nanoisland (20 × 13 nm^2, V_s = −1400 mV, and I_t = 10 pA). Lower panel: height profile along the arrow in the upper panel. (D) Schematic illustration of the Co intercalation, which is the metalation process route no. 5.

which about 6200 Co atoms were deposited on about 100 TPP molecules. Compared to Figure 2, the observations in Figure 3A were drastically changed. Only one well-ordered square island remained (marked by a dotted rectangle), while 90% of the molecules are disordered or decomposed into isolated molecules. Further, as also shown in Figure 3A, Co deposition alters the appearance of large fraction of 2HTPP molecules, which are classified into three types, labeled I, II, and III in Figure 3A. The type-I molecule was characterized by four-lobed shapes corresponding to phenyl groups with a slightly brighter spot at the center of the molecule. With respect to the type-II molecules, four phenyl groups appear slightly dark relative to type-I, and a brighter spot resides in the off-center position. With respect to the type-III molecules, four phenyl groups exhibited similar intensity with type-II while the center of the molecule appeared as characteristic four lobes alignment. The height profiles across the aforementioned three types of molecules along the arrows in Figure 3A exhibit a comparable height from the substrate: I, 0.32 nm; II, 0.36 nm; and III, 0.32 nm (Figure 3A, right panels), which are ∼0.1 nm higher than 2HTPP single molecule (∼0.22 nm). The experimental results suggest that type I, II, and III are not pure 2HTPP and instead correspond to incorporated Co atom inside via the route no. 1 or route no. 3 in Figure 1 with different appearances, which can be attributed to differently coordinated Co-2HTPP complexes. However, gentle adsorption via route no. 1 cannot explain the decomposition of the well-ordered molecular array. Route no. 3 could be the cause of the decomposition. At 300 K, the TPP molecules located at the edge of the island diffuse,[3] which provides an opportunity to meet with a diffusing 3d atom and

https://dx.doi.org/10.1021/acs.jpcc.9b09795
J. Phys. Chem. C 2020, 124, 3621−3631

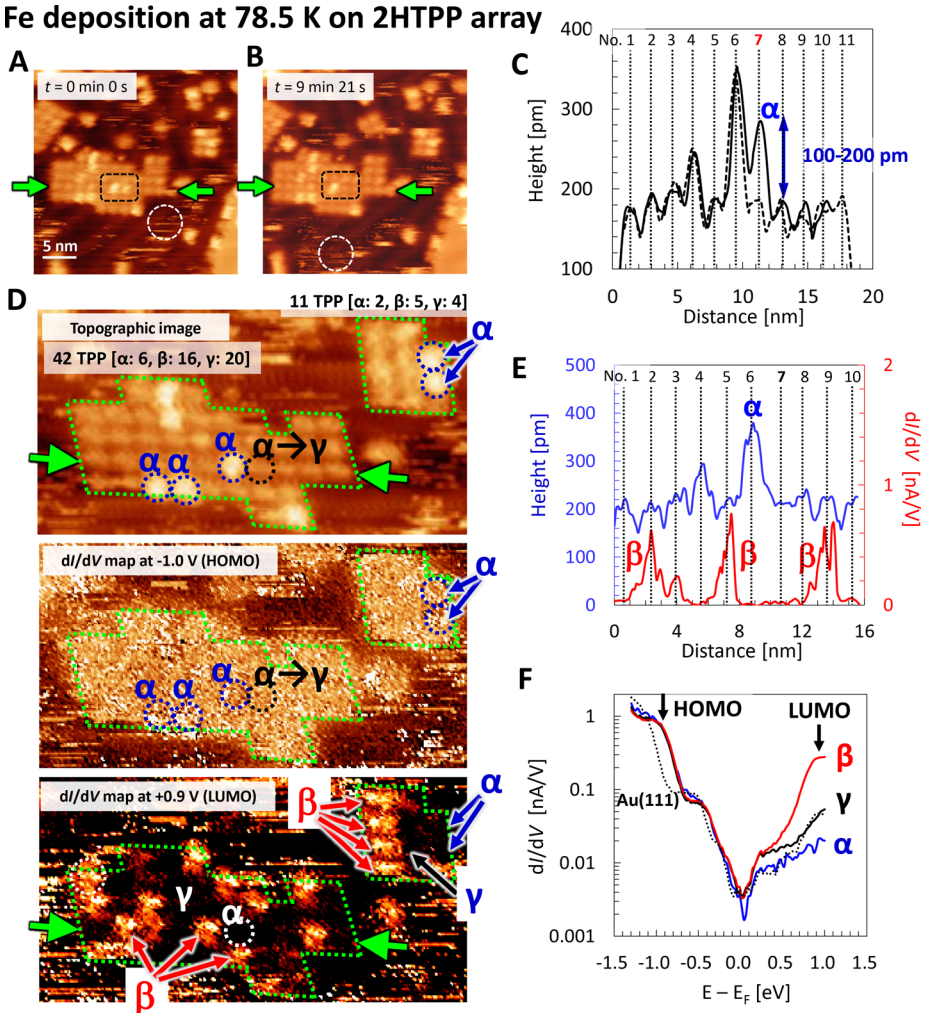

Figure 4. Fe deposition at 78.5 K on 2HTPP array in UHV. STM images are obtained at 78.5 K. (A, B) STM topography images obtained at the same area at different times: t = 0 min 0 s and t = 9 min 21 s (30 × 30 nm^2, V_s = −1400 mV, and I_t = 200 pA). Between two images, one of two bright spots denoted by the box is manipulated by the STM tip. (C) Height profiles between two green arrows in parts A and B before (solid line) and after (dashed line) the manipulation. (D) Scanning tunneling spectroscopy results (30 × 15 nm^2, V_s = −1400 mV, and I_t = 500 pA). At each pixel position, topography and dI/dV curves are simultaneously measured. Obtained STM topography and dI/dV maps at HOMO (−1.0 eV) and LUMO (+0.9 eV) are shown. Three different observations (α, β, and γ states) are found. (E) Line profiles of height (blue) and dI/dV intensity (red) between two green arrows marked in the STM topographic image and the dI/dV LUMO map in part D. (F) dI/dV curves obtained on the α [blue line], β [red line], γ state [black line], and the Au(111) substrate [dotted line].

form a Co-2HTPP complex. Once the Co-2HTPP was generated, the molecules stop diffusion; thus, the molecular array gradually decomposed.

It should be noted that about 6200 Co atoms were deposited on about 100 TPP molecules in Figure 3A, but we did not see any isolated Co atoms on the Au(111) terraces, which means that all of deposited Co atoms must be placed inside the TPP molecules, producing a variety of Co-2HTPP complexes with different numbers of metal atoms or intercalating below the molecules.

The indication of the intercalation is visible in Figure 3A, which is marked by a dotted triangle. Figure 3C shows one of the triangular-shaped islands (dotted lines are guides for eyes showing a 60° angle), while the triangular-shaped islands are not observed in Figure 2. Namely, the triangular island was caused by Co adsorption. It is well-known that the 3d metal deposition on fcc(111) substrate at 300 K forms triangular-shaped bilayer islands,[20,49,58,59] which indicates high diffusivity of the adsorbed 3d atoms on a closed packed fcc(111) surface at room temperature. One interesting point is that we frequently observed an atomically flat area at approximately the center of the island, and TPP molecules were located on the step edge of the island. The height profile across the island consisted of two layers (see Figure 3C). The atomically flat area exhibited a height of approximately 280 pm (marked by the arrow), which is half of the height of bilayer Co nanoislands on Au(111): ∼550 pm, thereby indicating the first layer of the island consisted of Co atoms. The single molecule located on the triangular island exhibited a height of approximately 200 pm, which was comparable to the height of 2HTPP on Au(111): ∼220 pm.

If one 2HTPP can hold only one atom inside, then excess Co atoms diffuse at 300 K on the surface until Co meets another Co. Once they form Co dimers, they continuously grow and form Co monolayer triangular-shape island following the substrate fcc-Au(111) 3-fold symmetry. The growth of the triangular-shaped island during the metalation indicated the existence of the route no. 5 (see Figure 3D). The DFT

https://dx.doi.org/10.1021/acs.jpcc.9b09795
J. Phys. Chem. C 2020, 124, 3621−3631

calculations indicated that on the noble metal substrate, the [π-conjugated molecule on 3d-atom] system was energetically significantly stable (~4 eV) when compared to the [3d-atom on π-conjugated molecule] system.[60] Therefore, it is energetically suitable for the adsorbed Co atoms to place below the molecule. The Co atoms inside three Co-2HTPP complexes in Figure 3A can be located below the 2HTPP molecules. Additionally, the formation of the Co-induced triangular-shape island suggested that adsorbed Co atoms not only preferred to be located below the molecule but also nucleated and formed the Co monolayer island.

An observation is that the TPP molecules were located on the island rim. Following the nucleation of 3d atoms and further island formation, the diffusing TPP molecules contact to the Co island edge. Subsequently, TPP molecules are placed on the Co and TPP diffusion stops. Therefore, the TPP molecules are located on the island rim. This also indicates a lower surface energy of the molecules when compared to that of metals: Co (2550 mJ/m^2) or Au (1550 mJ/m^2).[61]

As a result, the 300 K metalation can be categorized into two different regimes. First, when the number of deposited 3d metal atoms is less than the number of preadsorbed molecules, 3d atoms are inserted into the molecules one by one and subsequent annealing (at 350−700 K) successfully produces 3dTPP complexes while keeping the well-ordered molecular array, as reported before.[1] Second, however, when there are much more 3d metal atoms than preadsorbed molecules, a variety of metalation processes occur: (1) 3dTPP complex array with the original well-ordered square array structure remaining (only 10%), (2) isolated 3dTPP complexes (we confirmed at least three types) (80%), and (3) 3dTPP complexes placed on an intercalated 3d metal monolayer island (10%).

3.3. Iron Deposition at 78.5 K on 2HTPP Array. As shown in Figure 3, the metalation processes at 300 K provide a variety of 3dTPP complexes and strong 3d metal interactions change the morphology and form three types of new molecular structures, namely, (1) isolated clusters, (2) 3d metal intercalation, and (3) well-ordered 3dTPP array. Since these could be due to the thermal diffusion of the deposited 3d metal atoms at 300 K, we demonstrated an STM study on well-ordered square-shape 2HTPP molecular arrays (about 50 molecules) with an adsorption of about 100 Fe atoms at the substrate temperature maintained at 78.5 K. Interestingly, at the cryogenic temperature, previous X-ray photoemission spectroscopy results[44,50] suggested the precursor adcomplex state of Fe-2HTPP instead of FeTPP formation.

Figure 4A shows the resulting STM image. In contrast to Figure 3: the case of 3d-metal deposition at 300 K, 2HTPP islands were observed to maintain their square shapes (no triangular shaped islands were observed). Currently, we focused on an island located at the center of the image in Figure 4A. On the island, brighter spots marked by the box can be observed. Height profile between two green arrows in Figure 4A is denoted as a black line in Figure 4C. Eleven molecules (nos. 1−11) were placed. no. 6 and no. 7 molecules are 100−200 pm higher than other molecules. The results indicated that the brighter spots can correspond to adsorbed Fe atoms on 2HTPP. Figure 4B is obtained after 9 min 21 s at the same area as Figure 4A wherein eight brighter spots decreased to seven. Specifically, we manipulated one of the two brighter spots (no. 7) as denoted by the dotted box by closing the STM tip apex. The height profile between two green arrows in Figure 4B is shown as the dotted line in Figure 4C where the height of the no. 7 molecule evidently decreases from 280 to 180 pm. The STM demonstrations in Figure 4A−C indicate a weak bonding between the Fe atom and 2HTPP located below, thereby suggesting physisorption. The brighter spots are denoted as "α" spots.

Additionally, we observe a scratch-like noise [denoted by dotted circles in Figure 4, parts A and B] surroundings of the 2HTPP island, which was not observed on the surface in Figure 3. The scratches indicate that excess isolated Fe atoms remain on the flat bare Au terraces. At the cryogenic temperature, Fe atoms stay on the terrace, while they can be manipulated by the STM tip, which are known to be observed as the scratches in the STM topography.

The local density of states (LDOS) of Fe-adsorbed TPP islands at 78.5 K was measured using CITS method (see Methods). Figure 4D shows simultaneously obtained a topographic image and dI/dV maps at the highest occupied molecular orbital (HOMO) states: −1.0 eV and the lowest unoccupied molecular orbital (LUMO) states: + 0.9 eV, where the 0 eV denotes the Fermi energy, obtained from the same square TPP island. The full CITS and the dI/dV data are given in Figures S1 and S2, respectively. The differential conductance: dI/dV is proportional to sample LDOS, and thus the contrast in the dI/dV map denotes differences in LDOS at each atomic position of the sample surface.

The dI/dV map at −1.0 eV in Figure 4D shows clearly brighter areas, which correspond to the TPP molecule island location, thereby indicating a presence of the HOMO states. In the map, the "α" spot position appears no clear difference in contrast (see the dotted circles), thereby indicating no significant difference in LDOS at the "α" spot. However, significant new spots [named "β"] suddenly appeared when the dI/dV maps were checked at the LUMO state. The dI/dV map at +0.9 eV in Figure 4D shows clear 12 brighter spots in the island (pointed by red arrows "β").

Figure 4E shows the height profile [blue line] and dI/dV intensity profile [red line] obtained from the identical line as denoted by two green arrows in the topographic image and the dI/dV maps at +0.9 eV in Figure 4D. We identified the molecule positions corresponding to no. 1−10 from the height line profile. The "α" spot was confirmed only at the no. 6 molecule position with the apparent height corresponding to approximately 0.2 nm. However, along the line, three "β" spots were observed at molecules no. 2, no. 5, and no. 9, where approximately 1 nA/V higher dI/dV intensity was observed, albeit an almost negligible dI/dV value was confirmed at the no. 6 molecular position ("α"). Specifically, it is not possible to identify "β" in the topography. The experimental results clearly suggest "α" and "β" spots can be caused by different origins.

Namely, these STM topography images and dI/dV maps tell us that Fe deposition on 2HTPP array at 78.5 K produces three types of TPP complexes. (1) "α" state: an Fe atom weakly bonded on a 2HTPP (physisorption). (2) "β" state: no significant change in the topography, but a clear difference in LDOS. (3) "γ" state: TPP molecules which do not belong to neither "α" nor "β". In Figure 4D, the larger island (total 42 TPP) consists of 6 "α", 16 "β", and 20 "γ" and the smaller island (total 11 TPP) consists of 2 "α", 5 "β", and 4 "γ", which indicate that the majority are "β" and "γ" states.

dI/dV curves obtained at "α" [blue line], "β" [red line], and "γ" [black line] states are shown in Figure 4F, where E_F denotes the Fermi energy. The Au(111) curve [dotted line]

https://dx.doi.org/10.1021/acs.jpcc.9b09795
J. Phys. Chem. C 2020, 124, 3621−3631

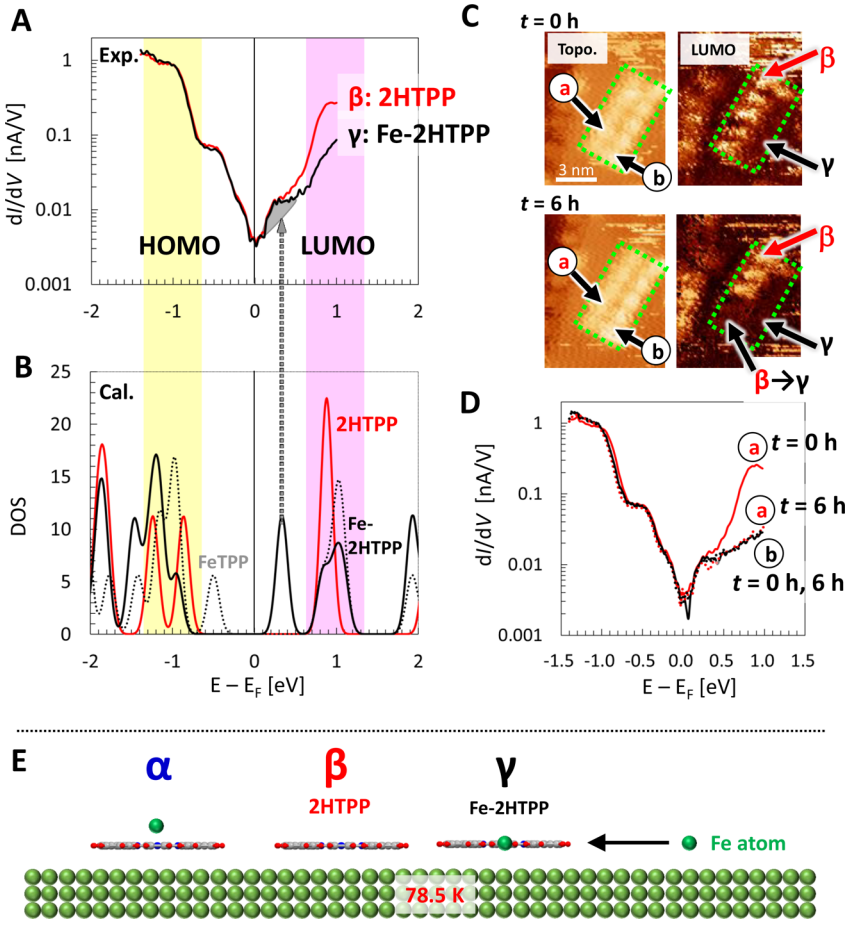

Figure 5. Fe-2HTPP adcomplex states at 78.5 K. (A) dI/dV curves obtained on the β [red line] and γ state [black line]. (B) Calculated density of states (DOS) of 2HTPP [red line] and Fe-2HTPP [black line]. Dotted line denotes FeTPP DOS. (C) Fe atom insertion into 2HTPP molecules during the STM measurement. Upper and lower panels denote STM topographic image and LUMO dI/dV maps at +0.9 eV before (t = 0 h) and after (t = 6 h) the insertion, respectively. (D) dI/dV curves obtained at the positions a [red lines] and b [black lines] in part C before (t = 0 h, solid line) and after (t = 6 h, dashed line) the insertion. (E) Schematic illustration of "α", "β", and "γ" states.

shows the Shockley surface states at approximately −0.5 eV.[53,62,63] On 2HTPP island, clear HOMO states at approximately −1.0 eV and LUMO states approximately +1.0 eV can be identified. These energy positions are good agreement with the previously reported HOMO/LUMO peaks positions for 2HTPP.[64,65] The origin of the −1.0 eV HOMO peaks are confirmed also by the dI/dV map obtained at −1.0 eV as shown in Figure 4D. Clear differences between "α", "β", and "γ" states are observed at the positive bias side in Figure 4F. The "β" state has a larger dI/dV intensity peak compared to "α" and "γ", and the "α" and "γ" states show similar curves.

Figure 5A shows dI/dV curves of the majority states of "β" [red line] and "γ" [black line] states, which can be compared with the calculated LDOS of 2HTPP and Fe-2HTPP adcomplex as shown in Figure 5B. One should be noted that the dI/dV curve of the "γ" state shows a clear shoulder peak (shaded area) around +0.3 eV in Figure 5A.

Figure 5B shows the theoretical free molecule DOS of 2HTPP [red line], Fe-2HTPP adcomplex [black solid line] and FeTPP [black dotted line]. Details of the calculated DOS of 2HTPP, Fe-2HTPP, and FeTPP are shown in the Supporting Information, Figure S3.The Fermi-level is set to the center of the HOMO−LUMO gap of 2HTPP (3.2 eV below the calculated vacuum level). The calculated LDOS reproduces well the HOMO and LUMO peaks of 2HTPP around −1 and +1 eV, respectively. For FeTPP and Fe-2HTPP, the same energy scale was used, such that the main molecular levels are well aligned between all three molecules. For Fe-2HTPP, this definition of the Fermi level (E_F) implies that the level at E_F + 0.3 eV is actually occupied in the free molecule calculation. In the real Fe-2HTPP/substrate system, it is quite possible that Fe is in a Fe^{2+} state, and the weakly bound Fe-4s electrons are transferred to the metal substrate. In the Fe-2HTPP DOS, the LUMO peak (at +0.9 eV in 2HTPP) is split into two peaks at 0.3 and 1 eV. The lower peak fits well the first peak at 0.3 eV in the experimental curves (the shaded-peak shoulder in Figure 5A) and the main LUMO peak at 1 eV has much lower intensity than the LUMO peak of 2HTPP. The large intensity difference around 1 eV agrees well with the experimental data and suggests that "β" and "γ" molecules correspond to 2HTPP and Fe-2HTPP, respectively.

Further, we calculated the DOS of two types of Fe-2HTPP adcomplex (see Supporting Information, Figure S4); Type A [black line in Figure S4]: two hydrogen atoms at the core position point upward. Type B [gray line in Figure S4]: one of the two hydrogen atoms at the core position points upward, while other points downward. Since both types of Fe-2HTPP adcomplex showed similar DOS, we used the DOS of the type A in Figure 5B.

https://dx.doi.org/10.1021/acs.jpcc.9b09795
J. Phys. Chem. C 2020, 124, 3621−3631

The DFT calculations show that the Fe-2HTPP adcomplex state is unstable against dehydrogenation; i.e., Fe-2HTPP is 1.6 eV higher in energy than FeTPP + H_2. Our STM experimental data exhibits that this type of metastable state can be produced at cryogenic temperatures.

Parts A and B of Figure 5 indicate that the experimentally observed the "β" state could be the 2HTPP without Fe insertion, while the "γ" state could be the Fe-2HTPP adcomplex state. Since the "α" state has similar LDOS as the "γ" state, these "α" and "γ" states could be Fe-2HTPP adcomplex states, while the difference was observed only in the topology: "α" is about 100−200 higher in height. Note that we succeeded to manipulate the "α" state between Figure 4A and 4B. Remarkably after the manipulation, the "α" state changed to "γ" state. This indicates that using the STM tip the physisorbed Fe atom could be inserted into the molecule. The STM observations of "α" and "γ" suggest there are at least two types of Fe-2HTPP adcomplex states during the cryogenic temperature metalation process.

Another significant point is that state switching from "β" to "γ" was observed during the STM measurement. All the STM topographic images shown in this manuscript were measured at −1.4 eV (HOMO states), no significant difference was observed in the topographic images between "β" and "γ" states. Figure 5C shows a rectangle-shape island in consist of ten TPP molecules. From the STM topographic image and the LUMO map, we identify the island includes six "β" (=2HTPP) and four "γ" states (=Fe-2HTPP). The upper panels in Figure 5C were obtained at t = 0 h, but after 6 h, the observations changed as depicted in the lower panels in Figure 5C. Now the same island consists of four "β" (=2HTPP) and six "γ" states (=Fe-2HTPP). Namely, during the STM observation, Fe atoms located on the terrace was inserted into the 2HTPP via the route no. 4 and formed the precursor adcomplex. This state switching was clearly visible in the dI/dV curves as shown in Figure 5D, where the dI/dV curves obtained at positions a and b are shown. Solid and dotted lines denote before (t = 0 h) and after (t = 6 h) the state switching. The dI/dV curves obtained at the position b [black line] are identical to those for the "γ" state for all time, but the dI/dV curves obtained at position a [red line] clearly shows the LDOS change from 2HTPP to Fe-2HTPP adcomplex state.

In summary, the present study of cryogenic temperature (78.5 K) deposition of the Fe atom (∼100 atoms) on a 2HTPP molecular array (∼50 molecules) has provided three important insights. (1) No significant change was observed in the molecular morphology after the Fe deposition at 78.5 K on 2HTPP array, which preserved the original well-ordered molecular structures in contrast to the 300-K metalation process. (2) In spite of the fact that we deposited about twice as many Fe atoms as 2HTPP molecules, about 40% (=21/53 in Figure 4D) of the TPP molecules remain as 2HTPP without Fe atom insertion, which indicates that the on-surface metalation process no. 1 dominates at cryogenic temperatures. (3) Two types of precursor adcomplex Fe-2HTPP states were observed. One could be the physisorbed Fe atom located on the 2HTPP (15% in Figure 4D), and the other could be the Fe atom inserted into the 2HTPP (45% in Figure 4D), while the Fe insertion into the 2HTPP is still processing during the STM measurements. The model in Figure 5E shows the summary of the possible produced adcomplexes.

4. CONCLUSIONS

On-surface metalation in UHV produces metal atom array following a well-ordered molecular platform with extreme lower concentration of impurity, which can be useful as a building block of designing 1 nm-size nanodevice and 1D- or 2D-lattice networks, and a precursor for further on-surface synthesis. In the study, direct imaging during the cryogenic temperature on-surface metalation process was successfully performed using the home-built low-temperature UHV STM setup. Fe deposition on 2HTPP array and STM/STS measurements were done at the sample temperature maintained at 78.5 K (about 100 Fe atoms on about 50 molecules). STM topographic images and HOMO/LUMO maps combined with DFT calculations unveiled the cryogenic temperature on-surface metalation process and identified three types of TPP appearance: (1) original 2HTPP (40%), (2) 2HTPP with an Fe atom on top (precursor adcomplex "α" state, 15%), and (3) 2HTPP with an Fe atom inside (precursor adcomplex "γ" state, 45%).

■ ASSOCIATED CONTENT

Supporting Information

The Supporting Information is available free of charge at https://pubs.acs.org/doi/10.1021/acs.jpcc.9b09795.

Figure S1, tunneling current maps of Fe atom adsorption on 2HTPP at 78.5 K in UHV; Figure S2, differential conductance maps (dI/dV maps) of Fe atom adsorption on 2HTPP at 78.5 K in UHV; Figure S3, DFT calculation results of 2HTPP, FeTPP, and Fe-2HTPP adcomplex; Figure S4, DFT calculation results of two types of Fe-2HTPP adcomplex; and Figure S5, STM topographic images of one ML H_2Pc film grown on Cu(111) before and after the 0.1 ML Fe deposition at 300 K in UHV (PDF)

■ AUTHOR INFORMATION

Corresponding Authors

Eiichi Inami − *Department of Materials Science, Chiba University, Chiba 263-8522, Japan; School of Systems Engineering, Kochi University of Technology, Kochi 782-8502, Japan;* orcid.org/0000-0002-2167-8510; Phone: +81-887-57-2307; Email: inami.eiichi@kochi-tech.ac.jp

Toyo Kazu Yamada − *Department of Materials Science and Molecular Chirality Research Center, Chiba University, Chiba 263-8522, Japan;* orcid.org/0000-0001-5185-6472; Phone: +81-43-290-3915; Email: toyoyamada@faculty.chiba-u.jp

Authors

Masataka Yamaguchi − *Department of Materials Science, Chiba University, Chiba 263-8522, Japan*

Ryohei Nemoto − *Department of Materials Science, Chiba University, Chiba 263-8522, Japan*

Hideki Yorimitsu − *Department of Chemistry, Graduate School of Science, Kyoto University, Kyoto 606-8502, Japan;* orcid.org/0000-0002-0153-1888

Peter Krüger − *Department of Materials Science and Molecular Chirality Research Center, Chiba University, Chiba 263-8522, Japan;* orcid.org/0000-0002-1247-9886

Complete contact information is available at: https://pubs.acs.org/10.1021/acs.jpcc.9b09795

https://dx.doi.org/10.1021/acs.jpcc.9b09795
J. Phys. Chem. C 2020, 124, 3621−3631

Notes

The authors declare no competing financial interest.

■ ACKNOWLEDGMENTS

This work was supported by JSPS KAKENHI Grant Numbers 19H05789, 17K19023 15K13357, 15H03531, 15H06092, 25110011, and 25600012, and the Murata Science Foundation. We thank Professor Dr. Hisao Ishii (Chiba University) for sublimation purification of 2HTPP molecules, Mr. Mikio Shimasaki for sublimation control of 2HTPP molecules, and Prof. Dr. Kohji Nakamura (Mie University) for supporting calculations.

■ REFERENCES

(1) Gottfried, J. M. Surface Chemistry of Porphyrins and Phthalocyanines. *Surf. Sci. Rep.* **2015**, *70*, 259−379.
(2) Krull, C.; Castelli, M.; Hapala, P.; Kumar, D.; Tadich, A.; Capsoni, M.; Edmonds, M. T.; Hellerstedt, J.; Burke, S. A.; Jelinek, P.; et al. Iron-Based Trinuclear Metal-Organic Nanostructures on a Surface with Local Charge Accumulation. *Nat. Commun.* **2018**, *9*, 3211.
(3) Inami, E.; Shimasaki, M.; Yorimitsu, H.; Yamada, T. K. Room Temperature Stable Film Formation of π-Conjugated Organic Molecules on 3d Magnetic Substrate. *Sci. Rep.* **2018**, *8*, 353.
(4) Bonifazi, D.; Kiebele, A.; Stöhr, M.; Cheng, F.; Jung, T.; Diederich, F.; Spillmann, H. Supramolecular Nanostructuring of Silver Surfaces via Self-Assembly of [60] Fullerene and Porphyrin Modules. *Adv. Funct. Mater.* **2007**, *17*, 1051−1062.
(5) Beletskaya, I.; Tyurin, V. S.; Tsivadze, A. Y.; Guilard, R.; Stern, C. Supramolecular Chemistry of Metalloporphyrins. *Chem. Rev.* **2009**, *109*, 1659−1713.
(6) Arnold, D.; Manno, D.; Micocci, G.; Serra, A.; Tepore, A.; Valli, L. Gas-Sensing Properties of Porphyrin Dimer Langmuir−Blodgett Films. *Thin Solid Films* **1998**, *327*, 341−344.
(7) Tepore, A.; Serra, A.; Manno, D.; Valli, L.; Micocci, G.; Arnold, D. P. Kinetic Behavior Analysis of Porphyrin Langmuir−Blodgett Films for Conductive Gas Sensors. *J. Appl. Phys.* **1998**, *84*, 1416−1420.
(8) Spadavecchia, J.; Ciccarella, G.; Siciliano, P.; Capone, S.; Rella, R. Spin-Coated Thin Films of Metal Porphyrin−Phthalocyanine Blend for an Optochemical Sensor of Alcohol Vapours. *Sens. Actuators, B* **2004**, *100*, 88−93.
(9) Kim, J.; Lim, S.-H.; Yoon, Y.; Thangadurai, T. D.; Yoon, S. A Fluorescent Ammonia Sensor based on a Porphyrin Cobalt (II)−Dansyl Complex. *Tetrahedron Lett.* **2011**, *52*, 2645−2648.
(10) Wang, L.; Li, H.; Deng, J.; Cao, D. Recent Advances in Porphyrin-Derived Sensors. *Curr. Org. Chem.* **2013**, *17*, 3078−3091.
(11) Cirera, B.; Björk, J.; Otero, R.; Gallego, J.; Miranda, R.; Ecija, D. Efficient Lanthanide Catalyzed Debromination and Oligomeric Length-Controlled Ullmann Coupling of Aryl Halides. *J. Phys. Chem. C* **2017**, *121*, 8033−8041.
(12) Meunier, B. Metalloporphyrins as Versatile Catalysts for Oxidation Reactions and Oxidative DNA Cleavage. *Chem. Rev.* **1992**, *92*, 1411−1456.
(13) Gutierrez-Cerón, C.; Páez, M. A.; Zagal, J. H. Reactivity Descriptors for Iron Porphyrins and Iron Phthalocyanines as Catalysts for the Electrooxidation of Reduced Glutathione. *J. Solid State Electrochem.* **2016**, *20*, 3199−3208.
(14) Zhang, X.; Wu, Z.; Zhang, X.; Li, L.; Li, Y.; Xu, H.; Li, X.; Yu, X.; Zhang, Z.; Liang, Y.; et al. Highly Selective and Active CO_2 Reduction Electrocatalysts based on Cobalt Phthalocyanine/Carbon Nanotube Hybrid Structures. *Nat. Commun.* **2017**, *8*, 14675.
(15) Wang, M.; Torbensen, K.; Salvatore, D.; Ren, S.; Joulié, D.; Dumoulin, F.; Mendoza, D.; Lassalle-Kaiser, B.; Işci, U.; Berlinguette, C. P.; et al. CO_2 Electrochemical Catalytic Reduction with a Highly Active Cobalt Phthalocyanine. *Nat. Commun.* **2019**, *10*, 1−8.
(16) Walter, M. G.; Rudine, A. B.; Wamser, C. C. Porphyrins and Phthalocyanines in Solar Photovoltaic Cells. *J. Porphyrins Phthalocyanines* **2010**, *14*, 759−792.
(17) Röckert, M.; Franke, M.; Tariq, Q.; Lungerich, D.; Jux, N.; Stark, M.; Kaftan, A.; Ditze, S.; Marbach, H.; Laurin, M.; et al. Insights in Reaction Mechanistics: Isotopic Exchange during the Metalation of Deuterated Tetraphenyl-21, 23 D-Porphyrin on Cu(111). *J. Phys. Chem. C* **2014**, *118*, 26729−26736.
(18) Yamamoto, S.; Mori, S.; Wagner, P.; Mozer, A. J.; Kimura, M. A Novel Covalently Linked Zn Phthalocyanine-Zn Porphyrin Dyad for Dye-sensitized Solar Cells. *Isr. J. Chem.* **2016**, *56*, 175−180.
(19) Jurow, M.; Schuckman, A. E.; Batteas, J. D.; Drain, C. M. Porphyrins as Molecular Electronic Components of Functional Devices. *Coord. Chem. Rev.* **2010**, *254*, 2297−2310.
(20) Schmaus, S.; Bagrets, A.; Nahas, Y.; Yamada, T. K.; Bork, A.; Bowen, M.; Beaurepaire, E.; Evers, F.; Wulfhekel, W. Giant Magnetoresistance through a Single Molecule. *Nat. Nanotechnol.* **2011**, *6*, 185−189.
(21) Wäckerlin, C.; Tarafder, K.; Siewert, D.; Girovsky, J.; Hählen, T.; Iacovita, C.; Kleibert, A.; Nolting, F.; Jung, T. A.; Oppeneer, P. M.; et al. On-surface Coordination Chemistry of Planar Molecular Spin Systems: Novel Magnetochemical Effects Induced by Axial Ligands. *Chemical Science* **2012**, *3*, 3154−3160.
(22) Raval, H. N.; Sutar, D.; Rao, V. R. Copper (II) Phthalocyanine Based Organic Electronic Devices for Ionizing Radiation Dosimetry Applications. *Org. Electron.* **2013**, *14*, 1281−1290.
(23) Tse, A. K.-S.; Mak, K. W.; Chan, K. S. Synthesis of Novel Cobalt (III) Porphyrin- Phosphoryl Complexes. *Organometallics* **1998**, *17*, 2651−2655.
(24) Paddock, R. L.; Hiyama, Y.; McKay, J. M.; Nguyen, S. T. Co (III) Porphyrin/DMAP: an Efficient Catalyst System for the Synthesis of Cyclic Carbonates from CO_2 and Epoxides. *Tetrahedron Lett.* **2004**, *45*, 2023−2026.
(25) Monteiro, C. J.; Jesus, P.; Davies, M. L.; Ferreira, D.; Arnaut, L. G.; Gallardo, I.; Pereira, M. M.; Serpa, C. Control of the Distance between Porphyrin Sensitizers and the TiO_2 Surface in Solar Cells by Designed Anchoring Groups. *J. Mol. Struct.* **2019**, *1196*, 444−454.
(26) Kadish, K.; Smith, K. M.; Guilard, R. *The Porphyrin Handbook*; Elsevier, 2000; Vol. 3.
(27) Wang, F.-X.; Liu, Y.-D.; Pan, G.-B. Vapor Growth and Photoconductivity of Single-Crystal Nickel-Phthalocyanine Nanorods. *Mater. Lett.* **2011**, *65*, 933−936.
(28) Tang, Q.; Li, H.; He, M.; Hu, W.; Liu, C.; Chen, K.; Wang, C.; Liu, Y.; Zhu, D. Low Threshold Voltage Transistors Based on Individual Single-Crystalline Submicrometer-Sized Ribbons of Copper Phthalocyanine. *Adv. Mater.* **2006**, *18*, 65−68.
(29) Zhang, Y.; Hu, W. Field-Effect Transistor Chemical Sensors of Single Nanoribbon of Copper Phthalocyanine. *Sci. China, Ser. B: Chem.* **2009**, *52*, 751−754.
(30) Bai, Y.; Sekita, M.; Schmid, M.; Bischof, T.; Steinrück, H.-P.; Gottfried, J. M. Interfacial Coordination Interactions Studied on Cobalt Octaethylporphyrin and Cobalt Tetraphenylporphyrin Monolayers on Au(111). *Phys. Chem. Chem. Phys.* **2010**, *12*, 4336−4344.
(31) Siemeling, U.; Schirrmacher, C.; Glebe, U.; Bruhn, C.; Baio, J. E.; Arnadottir, L.; Castner, D. G.; Weidner, T. Phthalocyaninato Complexes with Peripheral Alkylthio Chains: Disk-like Adsorbate Species for the Vertical Anchoring of Ligands onto Gold Surfaces. *Inorg. Chim. Acta* **2011**, *374*, 302−312.
(32) Marbach, H.; Steinrück, H.-P. Studying the Dynamic Behaviour of Porphyrins as Prototype Functional Molecules by Scanning Tunnelling Microscopy Close to Room Temperature. *Chem. Commun.* **2014**, *50*, 9034−9048.
(33) Kim, H.; Chang, Y. H.; Lee, S.-H.; Kim, Y.-H.; Kahng, S.-J. Switching and Sensing Spin States of Co−Porphyrin in Bimolecular Reactions on Au (111) using Scanning Tunneling Microscopy. *ACS Nano* **2013**, *7*, 9312−9317.
(34) Ecija, D.; Trelka, M.; Urban, C.; Mendoza, P. d.; Mateo-Martı, E.; Rogero, C.; Martín-Gago, J. A.; Echavarren, A. M.; Otero, R.; Gallego, J. M.; et al. Molecular Conformation, Organizational

https://dx.doi.org/10.1021/acs.jpcc.9b09795
J. Phys. Chem. C 2020, 124, 3621−3631

Chirality, and Iron Metalation of Meso-Tetramesitylporphyrins on Copper (100). *J. Phys. Chem. C* **2008**, *112*, 8988−8994.
(35) Buchner, F.; Xiao, J.; Zillner, E.; Chen, M.; Röckert, M.; Ditze, S.; Stark, M.; Steinrück, H.- P.; Gottfried, J. M.; Marbach, H. Diffusion, Rotation, and Surface Chemical Bond of Individual 2 H-Tetraphenylporphyrin Molecules on Cu (111). *J. Phys. Chem. C* **2011**, *115*, 24172−24177.
(36) Ditze, S.; Stark, M.; Drost, M.; Buchner, F.; Steinrück, H.-P.; Marbach, H. Activation En- ergy for the Self-Metalation Reaction of 2H-Tetraphenylporphyrin on Cu (111). *Angew. Chem., Int. Ed.* **2012**, *51*, 10898−10901.
(37) Nowakowski, J.; Wäckerlin, C.; Girovsky, J.; Siewert, D.; Jung, T. A.; Ballav, N. Porphyrin Metalation Providing an Example of a Redox Reaction Facilitated by a Surface Reconstruction. *Chem. Commun.* **2013**, *49*, 2347−2349.
(38) Wang, C.; Fan, Q.; Hu, S.; Ju, H.; Feng, X.; Han, Y.; Pan, H.; Zhu, J.; Gottfried, J. M. Coordination Reaction between Tetraphenylporphyrin and Nickel on a TiO_2(110) Surface. *Chem. Commun.* **2014**, *50*, 8291−8294.
(39) Xiang, F.; Li, C.; Wang, Z.; Liu, X.; Jiang, D.; Leng, X.; Ling, J.; Wang, L. Direct Observation of Copper-Induced Metalation of 5,15-Diphenylporphyrin on Au(111) by Scanning Tunneling Microscopy. *Surf. Sci.* **2015**, *633*, 46−52.
(40) Denawi, H.; Koudia, M.; Hayn, R.; Siri, O.; Abel, M. On-Surface Synthesis of Spin Crossover Polymeric Chains. *J. Phys. Chem. C* **2018**, *122*, 15033−15040.
(41) Sperl, A.; Kröger, J.; Berndt, R. Controlled Metalation of a Single Adsorbed Phthalocyanine. *Angew. Chem., Int. Ed.* **2011**, *50*, 5294−5297.
(42) Pham, V. D.; Repain, V.; Chacon, C.; Bellec, A.; Girard, Y.; Rousset, S.; Abad, E.; Dappe, Y. J.; Smogunov, A.; Lagoute, J. Tuning the Electronic and Dynamical Properties of a Molecule by Atom Trapping Chemistry. *ACS Nano* **2017**, *11*, 10742−10749.
(43) Krull, C.; Robles, R.; Mugarza, A.; Gambardella, P. Site- and Orbital-Dependent Charge Donation and Spin Manipulation in Electron-Doped Metal Phthalocyanines. *Nat. Mater.* **2013**, *12*, 337.
(44) Shubina, T. E.; Marbach, H.; Flechtner, K.; Kretschmann, A.; Jux, N.; Buchner, F.; Steinrück, H. P.; Clark, T.; Gottfried, J. M. Principle and Mechanism of Direct Porphyrin Metalation: Joint Experimental and Theoretical Investigation. *J. Am. Chem. Soc.* **2007**, *129*, 9476−9483.
(45) Kretschmann, A.; Walz, M. M.; Flechtner, K.; Steinrück, H. P.; Gottfried, J. M. Tetraphenylporphyrin Picks Up Zine Atoms From a Silver Surface. *Chem. Commun.* **2007**, No. 6, 568−570.
(46) Li, Y.; Xiao, J.; Shubina, T. E.; Chen, M.; Shi, Z.; Schmid, M.; Steinrück, H. P.; Gottfried, J. M.; Lin, N. Coordination and Metalation Bifunctionality of Cu with 5, 10, 15, 20- Tetra (4-pyridyl) Porphyrin: Toward a Mixed-Valance Two-Dimensional Coordination Network. *J. Am. Chem. Soc.* **2012**, *134*, 6401−6408.
(47) Goldoni, A.; Pignedoli, C. A.; Di Santo, G.; Castellarin-Cudia, C.; Magnano, E.; Bondino, F.; Verdini, A.; Passerone, D. Room Temperature Metalation of 2H-TPP Monolayer on Iron and Nickel Surfaces by Picking Up Substrate Metal Atoms. *ACS Nano* **2012**, *6*, 10800−10807.
(48) Stroscio, J. A.; Pierce, D. T.; Dragoset, R. A.; First, P. Microscopic Aspects of the Initial Growth of Metastable FCC Iron on Au (111). *J. Vac. Sci. Technol., A* **1992**, *10*, 1981−1985.
(49) Yamada, T. K.; Gerhard, L.; Balashov, T.; Takács, A. F.; Wesselink, R. J.; Wulfhekel, W. Electric Field Control of Fe Nano Magnets: Towards Metallic Nonvolatile Data Storage Devices. *Jpn. J. Appl. Phys.* **2011**, *50*, No. 08LA03.
(50) Röckert, M.; Franke, M.; Tariq, Q.; Steinrück, H. P.; Lytken, O. Evidence for Precursor Adcomplex during the Metalation of 2HTPP with Iron on Ag(001). *Chem. Phys. Lett.* **2015**, *635*, 60−62.
(51) Inami, E.; Yamaguchi, M.; Yamaguchi, T.; Shimasaki, M.; Yamada, T. K. Controlled Deposition Number of Organic Molecules Using Quartz Crystal Microbalance Evaluated by Scanning Tunneling Microscopy Single-Molecule-Counting. *Anal. Chem.* **2018**, *90*, 8954−8959.
(52) Barth, J. V.; Brune, H.; Ertl, G.; Behm, R. J. Scanning Tunneling Microscopy Observations on the Reconstructed Au(111) Surface: Atomic Structure, Long-Range Superstructure, Rotational Domains, and Surface Defects. *Phys. Rev. B: Condens. Matter Mater. Phys.* **1990**, *42*, 9307−9318.
(53) Chen, W.; Madhavan, V.; Jamneala, T.; Crommie, M. F. Scanning Tunneling Microscopy Observation of an Electronic Superlattice at the Surface of Clean Gold. *Phys. Rev. Lett.* **1998**, *80*, 1469−1472.
(54) Yamada, T. K.; Abe, T.; Nazriq, N. M. K.; Irisawa, T. Electron-Bombarded ⟨110⟩-Oriented Tungsten Tips for Stable Tunneling Electron Emission. *Rev. Sci. Instrum.* **2016**, *87*, No. 033703.
(55) Yamagishi, Y.; Nakashima, S.; Oiso, K.; Yamada, T. K. Recovery of Nanomolecular Electronic States from Tunneling Spectroscopy: LDOS of Low-Dimensional Phthalocyanine Molecular Structures on Cu(111). *Nanotechnology* **2013**, *24*, 395704.
(56) Kresse, G.; Furthmuller, J. Efficient Iterative Schemes for *ab-initio* Total Energy Calculations using a Plane-Wave Basis Set. *Phys. Rev. B: Condens. Matter Mater. Phys.* **1996**, *54*, 11169.
(57) Panchmatia, P. M.; Sanyal, B.; Oppeneer, P. M. GGA + U Modeling of Structural, Electronic, and Magnetic Properties of Iron Porphyrin-Type Molecules. *Chem. Phys.* **2008**, *343*, 47−60.
(58) Mishra, P.; Qi, Z. K.; Oka, H.; Nakamura, K.; Komeda, T. Spatially Resolved Magnetic Anisotropy of Cobalt Nanostructures on the Au(111) Surface. *Nano Lett.* **2017**, *17*, 5843−5847.
(59) Madhavan, V.; Chen, W.; Jamneala, T.; Crommie, M.; Wingreen, N. S. Tunneling into a Single Magnetic Atom: Spectroscopic Evidence of the Kondo Resonance. *Science* **1998**, *280*, 567−569.
(60) Yamada, T. K.; Nakashima, S.; Satoru, S.; Yamaguchi, T.; Ohta, N.; Nakamura, K. Tuning Electronic States of Fe Atom using Molecular Ligand Fields: On-Surface Construction of Fe-Phthalocyanine Complexes with STM Manipulation. Submitted for publication, 2020.
(61) Miedema, A. R.; de Chatel, P. F.; de Boer, F. R. Cohesion in Alloys − Fundamentals of a Semi-Empirical Model. *Physica B+C* **1980**, *100B*, 1−28.
(62) Echenique, P.; Berndt, R.; Chulkov, E.; Fauster, T.; Goldmann, A.; Höfer, U. Decay of Electronic Excitations at Metal Surfaces. *Surf. Sci. Rep.* **2004**, *52*, 219−317.
(63) Kowalczyk, P.; Kozlowski, W.; Olejniczak, W.; Datta, P. STS Investigations of Temperature Dependence of Au(111) Surface State Energy Position. *Surf. Sci.* **2006**, *600*, 1604−1607.
(64) Mielke, J.; Hanke, F.; Peters, M. V.; Hecht, S.; Persson, M.; Grill, L. Adatoms underneath Single Porphyrin Molecules on Au(111). *J. Am. Chem. Soc.* **2015**, *137*, 1844−1849.
(65) Wang, W.; Pang, R.; Kuang, G.; Shi, X.; Shang, X.; Liu, P. N.; Lin, N. Intramolecularly Resolved Kondo Resonance of High-Spin Fe(II)-Porphyrin Adsorbed on Au(111). *Phys. Rev. B: Condens. Matter Mater. Phys.* **2015**, *91*, No. 045440.

https://dx.doi.org/10.1021/acs.jpcc.9b09795
J. Phys. Chem. C 2020, 124, 3621−3631